MATERIALS CHEMISTRY
FRONTIERS

RESEARCH ARTICLE

View Article Online
View Journal | View Issue

Cite this: *Mater. Chem. Front.*, 2023, 7, 2235

Tin-based organic–inorganic metal halides with a reversible phase transition and thermochromic response†

Gele Teri, Hao-Fei Ni, Qing-Feng Luo, Xiao-Ping Wang, Jun-Qin Wang, Da-Wei Fu * and Qiang Guo *

Received 30th January 2023,
Accepted 15th March 2023

DOI: 10.1039/d3qm00105a

rsc.li/frontiers-materials

Organic–inorganic hybrid metal halides have been extensively studied since they have excellent photoelectric properties, diverse constituents, and tunable band gaps. However, most of the discoveries are random and there is a lack of new systems to find something worth exploring. Here, we have successfully synthesized two tin-based organic–inorganic hybrid halides $(BPA)_2SnCl_6$ (**1**, BPA-Cl) and $(BPA)_2SnBr_6$ (**2**, BPA-Br) (BPA = 3-bromopropan-1-ammonium) with a reversible dielectric switching response using halogen modulation. Differential scanning calorimetry (DSC) and dielectric measurements determined the phase transition temperatures (T_c) to be **1** (284.24 K) and **2** (301.89 K), and the T_c increased with halogen ion size. According to the 2D fingerprinting of Hirshfeld surface plots, the short mean (di, de) also changes with the variation of the inorganic framework, which is in accordance with DSC and dielectric results. The UV-NIR-vis absorption spectra reveal that **1** is a direct bandgap semiconductor (2.97 eV) and **2** is an indirect bandgap semiconductor (2.66 eV). In addition, compound **2** exhibits a fascinating reversible thermochromic response. This work not only provides a new systematic approach to synthesizing dielectric materials, but also proposes a route to obtain narrow-bandgap optoelectronic semiconductors.

Introduction

Organic–inorganic metal halides have been attracting more research interest as key components in optical devices, solar cells, light-emitting diodes, and nonlinear optical materials.[1–10] The perfect combination of organic and inorganic components provides feasibility for the occurrence of phase transition behavior.[11–13] At the same time, dielectric phase transition (thermally stimulated response) materials often bring about interesting physical properties such as fluorescence,[14–16] thermochromism,[17–20] ferroelectricity[21–23] and so on.[24–30] Compared with high-dimensional hybrid phase transition materials with limited organic ammonium species, the structures of low-dimensional compounds are more flexible and diverse.[31–34] Meanwhile, low-dimensional materials can provide a large degree of freedom for organic ammonium, thereby triggering the order–disorder phase transition.[35–38] As an example, Zou *et al.* reported a zero-dimensional organic–inorganic hybrid single crystal $(TMA)_2SbCl_5$-DMF (TMA = $(CH_3)_3NH^+$, DMF = $HCON(CH_3)_2$) with a high quantum yield of 67.2%.[39] Zang *et al.* reported a zero-dimensional halogenated zinc organic hybrid $(H_2TTz)ZnCl_4$-MeOH (TTz = 2,5-bis(4-pyridinium)thiazolo[5,4-*d*]thiazole) with excellent optical waveguide properties.[40] In addition, our group synthesized the compound $(CASD)_2MnBr_4$ (CASD = 8-chloro-5-azonia-spiro [4.5] decane), which exhibits a large SHG response.[33]

Currently, most of the organic–inorganic phase transition perovskites reported are based on lead (Pb),[41–43] antimony (Sb),[37] bismuth (Bi),[44,45] cadmium (Cd),[46–48] and manganese (Mn).[49–51] In spite of this, there are still some problems associated with potential toxicity and environmental pollution, which limit the further applications of these materials.[8,14,52] Therefore, research into environmentally friendly lead-free zero-dimensional organic–inorganic metal halides is in full swing. Among them, tin-based zero-dimensional organic–inorganic hybrid materials have attracted significant interest as tin is located in the same group as lead and their electronic structures are both (ns^2np^2).[53] Therefore, tin-based materials have excellent optical properties.[19,54] Additionally, tin-based halides have also received attention due to their thermochromic properties.[19] In simple terms, the color of the material changes with temperature so it can be used as a temperature indicator or alarm.[55] To the best of our knowledge, there are

Institute for Science and Applications of Molecular Ferroelectrics, Key Laboratory of the Ministry of Education for Advanced Catalysis Materials, Zhejiang Normal University, Jinhua, 321004, People's Republic of China.
E-mail: dawei@zjnu.edu.cn, qiangguo@zjnu.edu.cn

† Electronic supplementary information (ESI) available: Experimental details, materials and methods, powder X-ray diffraction (PXRD), dielectric measurement, selected bond lengths and angles for compounds. CCDC 2231652–2231655. For ESI and crystallographic data in CIF or other electronic format see DOI: https://doi.org/10.1039/d3qm00105a

few reports on the thermochromic effect of tin-based halides, limited to our report on [2-(2-fluorophenyl)ethan-1-ammonium]$_2$SnBr$_6$, which has both thermochromic and ferroelastic properties.[19]

Above all, to investigate the effect of inorganic frameworks on physiochemical properties of organic–inorganic halides, (BPA)$_2$SnCl$_6$ (**1**) and (BPA)$_2$SnBr$_6$ (**2**) are designed by halogen modulation. Both compounds exhibit a zero-dimensional inorganic framework $[SnX_6]^{2-}$ (X = Cl, Br) with discrete organic $[BPA]^+$ cations. Satisfyingly, the phase transition temperature is elevated from 284.24 K to 301.89 K with the modulation of the halogen ion size. We find that both compounds exhibit reversible dielectric switching, while compound **2** shows a thermochromic response. In a word, this study provides new insights into zero-dimensional organic–inorganic halides, which might bring new ideas to optoelectronics.

Results and discussion

Structural analysis

To explain the origin of the phase transition, single-crystal X-ray diffraction was performed on compounds **1** and **2**. The powder X-ray diffraction (PXRD) spectra are in good agreement with the simulated spectra, indicating that the products are of high purity (Fig. S1, ESI†). At 273 K (LTP), compound **1** crystallizes in the space group $P2_1/c$ of the monoclinic crystal system with the following cell parameters: a = 10.715(5) Å, b = 7.267(2) Å, c = 12.829(5) Å, β = 109.487(6), and V = 941.8(6) Å^3 (Table S1, ESI†). The asymmetric unit consists of half of the inorganic framework $[SnCl_6]^{2-}$ and a $C_3H_9BrN^+$ cation, and thus the charge is balanced. From Table S3 (ESI†) it can be seen that the Sn atom is connected to six adjacent Cl atoms to form the $[SnCl_6]$ octahedron, the Cl–Sn–Cl bond angles are close to 90°and 180°, indicating that the $[SnCl_6]$ configuration is close to a regular octahedron. The Sn–Cl bond length varies from 2.4462(16) to 2.4538(18) Å, which is consistent with related reports.[19] At LTP, both cations and anions adopt an ordered state. The $[SnCl_6]$ octahedra are separated by discrete organic ammonium cations ($C_3H_9BrN^+$), forming a zero-dimensional structure. It is this zero-dimensional structure that provides sufficient degrees of freedom for the ions to move in a way that facilitates the order–disorder phase transition. At 300 K (HTP), compound **1** still crystallizes in the space group $P2_1/m$ of the monoclinic crystal system with the following cell parameters: a = 11.040(3) Å, b = 7.3622(15) Å, c = 12.282(3) Å, β = 105.063(6), and V = 964.0(4) Å^3. Compared with LTP, the N and C atoms of BPA^+ at HTP change to a two-fold disordered state. When the temperature reaches T_c, the disorder of organic ammonium brings about changes in bond lengths and bond angles. The geometric configuration of compound **1** alters drastically after this process, revealing its internal mechanism. The Sn–Cl bond length also transforms from 2.450 Å to 2.448 Å. The above results suggest that compound **1** undergoes an order–disorder phase transition from LTP to HTP (Fig. 1).

At 240 K (LTP), compound **2** crystallizes in the space group $P2_1/c$ of the monoclinic crystal system with the following cell parameters: a = 10.886(8) Å, b = 7.493(5) Å, c = 13.119(8) Å, β = 110.449(13), and V = 1002.7(12) Å^3 (Table S2, ESI†). Due to the larger radius of the bromine atom compared to the chlorine atom, the volume of **2** is also slightly larger than **1**. Since the LTP structures of compounds **1** and **2** are almost identical, the LTP structure of compound **2** is not discussed in detail. At 333 K (HTP), compound **2** still crystallizes in the space group $P2_1/m$ of the monoclinic crystal system with the following cell parameters: a = 11.0559(15) Å, b = 7.6425(6) Å, c = 12.6907(15) Å, β = 105.813(13), and V = 1031.7(2) Å^3. The asymmetric unit consists of half of the $[SnBr_6]^{2-}$ and a $C_3H_9BrN^+$ cation. At HTP, the organic ammonium cations are in a disordered state. The Sn–Br bond length varies between 2.575(3) and 2.586(5) Å (Table S4, ESI†). The inorganic frame of compound **2** also changes after the phase transition (Fig. 2 and Fig. S2, ESI†).

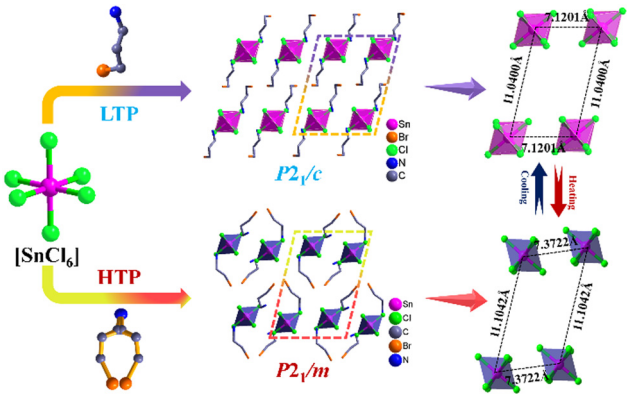

Fig. 1 A schematic diagram of the LTP and HTP structures in compound **1**. For clarity, all H atoms are omitted.

DSC and dielectric analyses

Generally speaking, dielectric and DCS measurements are favorable methods to detect phase transitions occurring in compounds. Therefore, DSC and dielectric measurements were

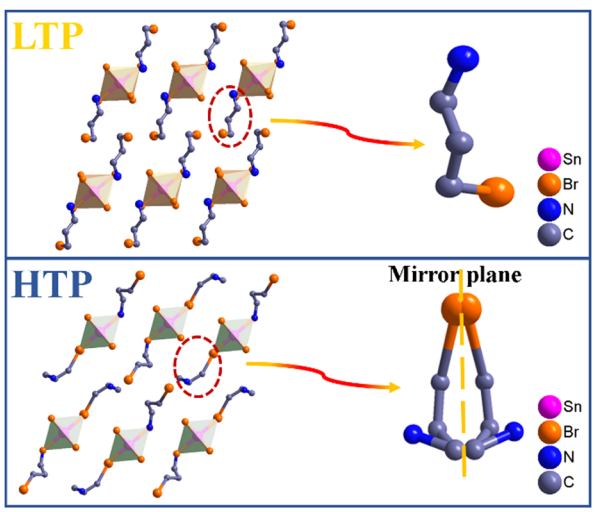

Fig. 2 Packing structures of the LTP and HTP in compound **2**. For clarity, all H atoms are omitted.

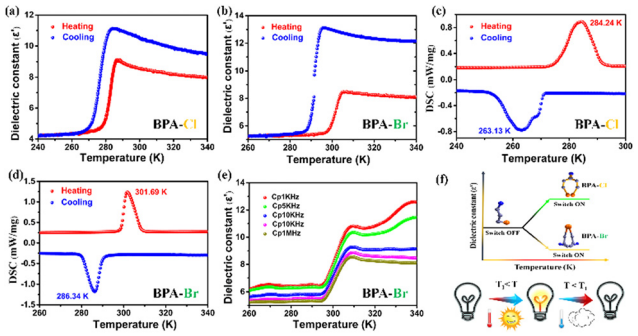

Fig. 3 (a and b) DSC curves of **1** and **2** in heating-cooling runs. (c and d) Dielectric constant of **1** and **2**. (e) The dielectric measurement of **2** at 1 kHz, 5 kHz, 10 kHz, 100 kHz and 1 MHz upon heating. (f) A schematic diagram of the molecular switch simulation based on thermosensitive signal conversion.

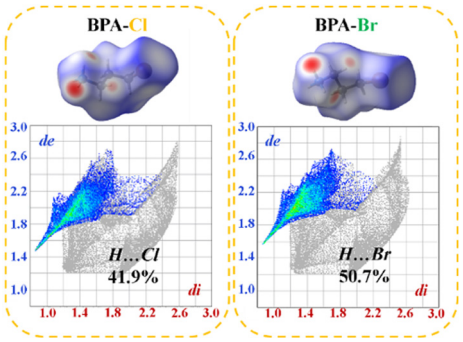

Fig. 4 Hirshfeld surfaces (top) and 2D fingerprint plots (bottom) for **1** and **2**.

performed on compounds **1** and **2** in the temperature range of 240–340 K. Two consecutive DSC cycles were performed on the powders of **1** and **2** (Fig. S3, ESI†). Fig. 3c and d shows that compound **1** undergoes a sudden change in dielectric constant at *ca.* 280 K (from 4 to 9) and the dielectric anomaly of compound **2** (from 5 to 9) occurs near 300 K. From the apparent change in dielectric constant, it can be tentatively concluded that the two compounds undergo a phase transition. Therefore, for further determination, DSC measurements were performed on the compounds. As shown in Fig. 3a and b, there are endothermic and exothermic peaks during heating and cooling, respectively. For compound **1**, a pair of endothermic/exothermic peaks with a thermal hysteresis of about 21 K (284.24 K/263.13 K) appears, and the entropy is 26.86 J mol^{-1} K^{-1}. For compound **2**, a pair of endothermic/exothermic peaks with a thermal hysteresis of about 16 K appears at about 301.89 K/286.34 K, and its entropy becomes 50.61 J mol^{-1} K^{-1}. Although the phase transition temperatures of compounds **1** and **2** are relatively close, compound **1** has a larger thermal hysteresis. The above results confirm that this process is accompanied by a first-order phase transition. Also, the real part of the dielectric constant (ε') of compounds **1** and **2** were measured at different frequencies (Fig. 3e and Fig. S4, ESI†). As the frequency decreases, ε' gradually increases, but the temperature at the maximum value of ε' remains almost constant at different measured frequencies, indicating that compounds **1** and **2** do not show any dielectric relaxation in the measured frequency range. The phase transition temperatures of both compounds are close to room temperature, making them good reversible dielectric switches without strict working conditions (Fig. 3f).

Hirshfeld surface and 2D-fingerprint analyses

To better understand the intermolecular interaction forces of the compound during the phase transition, the Hirshfeld surface and two-dimensional fingerprints were calculated using CrystalExplorer software. The different colors on the Hirshfeld surface represent the interactions between molecules: white represents the van der Waals distance, blue represents longer contacts and red represents closer contacts. As shown in Fig. 4, small changes in the contact surface occur when the inorganic framework is tuned. (di, de) for BPA-Cl, *i.e.* (1.6589, 1.9084), is smaller than that of BPA-Br (1.6589, 1.9799), which allows us to know that the interaction forces between cations and anions are different. In addition, compound **2** shows stronger hydrogen bonding due to the apparent contact of its cations indicated by the red circular grooves. These results are consistent with those obtained from the Hirshfeld surfaces and also demonstrate that compound **2** exhibits a higher phase transition temperature.

Semiconducting properties and reversible thermochromism

In addition, the semiconductor properties of the title compounds were characterized to investigate the effect of halogen modulation on the band gap. Fig. 5a shows that the absorption edge of BPA-Br (465 nm) is larger than that of BPA-Cl (423 nm). To better understand the relationship between the valence and conduction bands, analysis of the energy band structure and density of states was performed. Based on the position of the valence band maximum (VBM) and the conduction band minimum (CBM), it can be concluded that compound **1** is a direct semiconductor (3.00 eV), while compound **2** is an indirect semiconductor (2.09 eV) (Fig. 5b and e). This is more consistent with the results obtained from the Tauc curve (Fig. 5d) (**1**, 2.97 eV; **2**, 2.66 eV), indicating that halogen modulation has an effect on the band gap. As shown in Fig. 5c and f, the VBM and CBM are mainly contributed to by the inorganic part. Moreover, by comparing the band gap with those of other tin-based organic–inorganic hybrids (Fig. 6a), the title compounds belong to

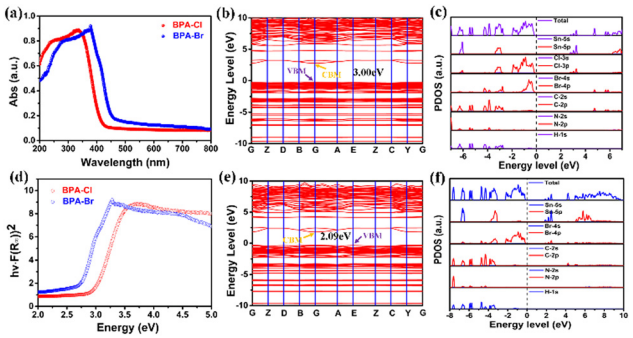

Fig. 5 (a) UV-NIR-vis absorption spectra of **1** and **2**. (b and e) Band structures of **1** and **2**. (c and f) Partial densities of states of **1** and **2**. (d) Optical band gaps of **1** and **2** as calculated by the Tauc equation.

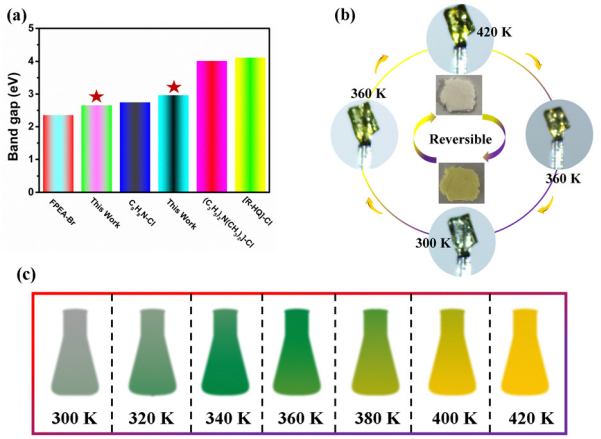

Fig. 6 (a) The band gap in this work compared with other tin-based organic–inorganic halides. (b) The temperature-induced color change in the crystal and powders of **2**. (c) A schematic of the reversible color change of **2**.

the narrower band gap semiconductors, indicating that they have a wide range of applications in optoelectronic devices (FPEA: 2-(2-fluorophenyl)ethan-1-ammonium;[19] FMBA: 3-fluoro-*N*-methylbenzylamine;[56] C_9H_8N: quinoline;[57] $C_{10}H_{20}ClN$: diallyldimethylaminium chloride;[58] *R*-HQ: (*R*)-3-hydroxyquinuclidinium;[53] TMIM: trimethyliodomethylammonium).[59]

Thermochromic materials have potential applications in the fields of anti-counterfeiting, sensors and smart windows. The thermochromic behaviour mostly reported is caused by the lattice change or ionic rearrangement. Surprisingly, the large crystal of compound **2** exhibits an excellent thermochromic response. As shown in Fig. 6b, compound **2** exhibits a light green color at 300 K. The color changes more significantly with increasing temperature, and it finally shows a dark green color at 420 K. Interestingly, the dark green color gradually returns to light green as the temperature decreases, indicating that compound **2** exhibits an interesting reversible thermochromic response. Additionally, the measured thermogravimetric (TG) results indicate that the decomposition temperatures of compounds **1** and **2** are much higher than the phase transition temperatures, ensuring their thermal stability for potential applications (Fig. S5, ESI†). This thermochromic behaviour is mainly caused by the deformation of $[SnBr_6]^{2-}$ octahedra during the structural phase transitions from LTP to HTP. It is a promising material to be applied in temperature sensors (Fig. 6c and Fig. S6, ESI†).

Conclusions

In summary, we have synthesized two tin-based organic–inorganic halides $(BPA)_2SnCl_6$ (**1**) and $(BPA)_2SnBr_6$ (**2**) by rational halogen modulation. The phase transition temperature gradually increases (284.24 → 301.89 K) with the increasing halogen ion size. Meanwhile, DSC and dielectric measurements further provide reliable evidence for this result. Furthermore, rational design of the band gap is realized, which guides us to discover more narrow band gap semiconductors. Compound **2** also exhibits a reversible thermochromic response for applications in temperature sensors and smart windows. This work could provide new ideas for the subsequent exploration of novel organic–inorganic hybrid halides.

Author contributions

G. Teri planned the experiments and drafted the manuscript. H. Ni performed the calculations and analysed the band structure. Q. Luo, Xiao. Wang and J. Wang assisted with determining the single crystal structures. Q. Guo conceived and directed this work. D. Fu supervised and provided suggestions for research. All authors contributed to the work in the manuscript.

Conflicts of interest

There are no conflicts to declare.

Acknowledgements

This work was financially supported by the Natural Science Foundation of Zhejiang Province (LZ20B010001) and the National Natural Science Foundation of China (grant 21991141).

Notes and references

1 M. Mączka, A. Gagor, J. K. Zaręba, D. Stefanska, M. Drozd, S. Balciunas, M. Šimėnas, J. Banys and A. Sieradzki, Three-Dimensional Perovskite Methylhydrazinium Lead Chloride with Two Polar Phases and Unusual Second-Harmonic Generation Bistability above Room Temperature, *Chem. Mater.*, 2020, **32**, 4072–4082.

2 C. F. Wang, H. Li, Q. Ji, C. Ma, L. Liu, H. Y. Ye, B. Cao, G. Yuan, H. F. Lu, D. W. Fu, M. G. Ju, J. Wang, K. Zhao and Y. Zhang, Discovery of a 2D Hybrid Silver/Antimony-Based Iodide Double Perovskite Photoferroelectric with Photostrictive Effect and Efficient X-Ray Response, *Adv. Funct. Mater.*, 2022, **32**, 2205918.

3 M. Mączka, J. K. Zaręba, A. Gągor, D. Stefańska, M. Ptak, K. Roleder, D. Kajewski, A. Soszyński, K. Fedoruk and A. Sieradzki, $[Methylhydrazinium]_2PbBr_4$, a Ferroelectric Hybrid Organic–Inorganic Perovskite with Multiple Nonlinear Optical Outputs, *Chem. Mater.*, 2021, **33**, 2331–2342.

4 X. L. Xu, L. B. Xiao, J. Zhao, B. K. Pan, J. Li, W. Q. Liao, R. G. Xiong and G. F. Zou, Molecular Ferroelectrics-Driven High-Performance Perovskite Solar Cells, *Angew. Chem., Int. Ed.*, 2020, **59**, 19974–19982.

5 H. F. Ni, L. K. Ye, P. C. Zhuge, B. L. Hu, J. R. Lou, C. Y. Su, Z. X. Zhang, L. Y. Xie, D. W. Fu and Y. Zhang, A nickel(II)-based one-dimensional organic–inorganic halide perovskite ferroelectric with the highest Curie temperature, *Chem. Sci.*, 2023, **14**, 1781–1786.

6 Q. Pan, Y.-A. Xiong, T.-T. Sha and Y.-M. You, Recent Progress in the Piezoelectricity of Molecular Ferroelectrics, *Mater. Chem. Front.*, 2021, **5**, 44–59.

7 Y. Ai, R. Sun, W. Q. Liao, X. J. Song, Y. Y. Tang, B. W. Wang, Z. M. Wang, S. Gao and R. G. Xiong, Unprecedented Ferroelectricity and Ferromagnetism in a Cr^{2+}-Based Two-Dimensional Hybrid Perovskite, *Angew. Chem., Int. Ed.*, 2022, **61**, e202206034.
8 C. Y. Su, Y. F. Yao, Z. X. Zhang, Y. Wang, M. Chen, P. Z. Huang, Y. Zhang, W. C. Qiao and D. W. Fu, The construction of a two-dimensional organic–inorganic hybrid double perovskite ferroelastic with a high T_c and narrow band gap, *Chem. Sci.*, 2022, **13**, 4794–4800.
9 Y. W. Zhang, Q. Wang, P. P. Shi, W. Y. Zhang, Q. Ye and D. W. Fu, Visual Low-high Interchange in Dielectric Switch for Trimethylchloroethylamine Tetrachlozincate with Large Leap Symmetry Breaking, *Mater. Chem. Front.*, 2019, **3**, 2077–2082.
10 C. Su, Z. Zhang, J. Yao, M. Chen, P. Huang, Y. Zhang, D. Fu and L. Xie, Construction, photoelectric response and phase transition for new hybrid double perovskites showing narrow band gaps, *Chin. Chem. Lett.*, 2023, **34**, 107442.
11 Q. Q. Jia, L. Tong, W. Y. Zhang, D. W. Fu and H. F. Lu, Two-Step Dielectric Responsive Organic–Inorganic Hybrid Material with Mid-Band Light Emission, *Chem. – Eur. J.*, 2022, **28**, e202200579.
12 T. Zhang, K. Xu, J. Li, L. He, D.-W. Fu, Q. Ye and R.-G. Xiong, Ferroelectric hybrid organic–inorganic perovskites and their structural and functional diversity, *Natl. Sci. Rev.*, 2023, **10**, nwac240.
13 J. Harada, M. Takehisa, Y. Kawamura, H. Takahashi and Y. Takahashi, Plastic/Ferroelectric Crystals with Distorted Molecular Arrangement: Ferroelectricity in Bulk Polycrystalline Films through Lattice Reorientation, *Adv. Electron. Mater.*, 2022, **8**, 2101415.
14 Q. Jia, T. Shao, L. Tong, C. Su, D. Fu and H. Lu, Lead-free bilayer heterometallic halide perovskite with reversible phase transition and photoluminescence properties, *Chin. Chem. Lett.*, 2023, **34**, 107539.
15 Y. Y. Tang, Y. L. Zeng and R. G. Xiong, Contactless Manipulation of Write-Read-Erase Data Storage in Diarylethene Ferroelectric Crystals, *J. Am. Chem. Soc.*, 2022, **144**, 8633–8640.
16 M. Rok, B. Zarychta, R. Janicki, M. Witwicki, A. Bienko and G. Bator, Dielectric-Optical Switches: Photoluminescent, EPR, and Magnetic Studies on Organic–Inorganic Hybrid $(azetidinium)_2MnBr_4$, *Inorg. Chem.*, 2022, **61**, 5626–5636.
17 J. C. Liu, W. Q. Liao, P. F. Li, Y. Y. Tang, X. G. Chen, X. J. Song, H. Y. Zhang, Y. Zhang, Y. M. You and R. G. Xiong, A Molecular Thermochromic Ferroelectric, *Angew. Chem., Int. Ed.*, 2020, **59**, 3495–3499.
18 A. Elattar, H. Suzuki, R. Mishima, K. Nakao, H. Ota, T. Nishikawa, H. Inoue, A. K. K. Kyaw and Y. Hayashi, Single crystal of two-dimensional mixed-halide copper-based perovskites with reversible thermochromism, *J. Mater. Chem. C*, 2021, **9**, 3264–3270.
19 T. Shao, H. F. Ni, C. Y. Su, Q. Q. Jia, L. Y. Xie, D. W. Fu and H. F. Lu, Integrated Reversible Thermochromism, High T_c, Dielectric Switch and Narrow Band Gap in One Multifunctional Ferroic, *Chem. – Eur. J.*, 2022, **28**, e202202533.
20 M. Wan, H.-R. Chen, Y.-N. Wang, K. Shi, J.-Y. Liu, Z.-M. Li, S.-Y. Ye, J.-Y. Li and L.-Z. Chen, Reversible thermochromism to tune the bandgap of organic–inorganic hybrid materials, *Mater. Chem. Front.*, 2022, **6**, 3094–3101.
21 L. P. Miao, N. Ding, N. Wang, C. Shi, H. Y. Ye, L. Li, Y. F. Yao, S. Dong and Y. Zhang, Direct observation of geometric and sliding ferroelectricity in an amphidynamic crystal, *Nat. Mater.*, 2022, **21**, 1158–1164.
22 X. Niu, L. Liang, X. Zhang, Z. Wang, T. Zhu, J. Wu, Q. Guan, L. Hua and J. Luo, Centimeter-sized single crystals of 2D hybrid perovskites toward ultraviolet photodetection with anisotropic photoresponse, *Mater. Chem. Front.*, 2022, **6**, 3598–3604.
23 H. Peng, J.-C. Qi and W.-Q. Liao, Optically Controlled Polarization Switching in an Organic Ferroelectric with Light- and Temperature-Triggered Phase Transitions, *Chem. Mater.*, 2022, **34**, 3067–3075.
24 A. G. Fernandez, J. M. B. Garcia, S. C. Garcia, A. L. L. Saiz, R. Artiaga, J. L. Beceiro, S. Hu, W. Ren, A. Stroppa, M. S. Andujar and M. A. S. Rodriguez, Phase Transition, Dielectric Properties, and Ionic Transport in the $[(CH_3)_2NH2]PbI_3$ Organic–Inorganic Hybrid with 2H-Hexagonal Perovskite Structure, *Inorg. Chem.*, 2017, **56**, 4918–4927.
25 T. Zhang, K. Ding, J. Y. Li, G. W. Du, L. L. Chu, Y. Zhang and D. W. Fu, Hydrogen-Bonded Engineering Enhancing Phase Transition Temperature in Molecular Perovskite Ferroelastic, *Chin. J. Chem.*, 2022, **40**, 1559–1565.
26 Z.-X. Zhang, C.-Y. Su, J.-X. Gao, T. Zhang and D.-W. Fu, Mechanochemistry enables optical-electrical multifunctional response and tunability in two-dimensional hybrid perovskites, *Sci. China Mater.*, 2020, **64**, 706–716.
27 H. Ye, X.-X. Chen, D.-X. Liu, B.-Q. Zhao, Y.-B. Li, Y. Zeng, W.-X. Zhang and X.-M. Chen, Subtly tuning intermolecular hydrogen bonds in hybrid crystals to achieve ultrahigh-temperature molecular ferroelastic, *Chem. Sci.*, 2022, **13**, 14124–14131.
28 J. Harada, T. Shimojo, H. Oyamaguchi, H. Hasegawa, Y. Takahashi, K. Satomi, Y. Suzuki, J. Kawamata and T. Inabe, Directionally tunable and mechanically deformable ferroelectric crystals from rotating polar globular ionic molecules, *Nat. Chem.*, 2016, **8**, 946–952.
29 Q.-Q. Jia, H.-F. Ni, M.-M. Lun, L.-Y. Xie, H.-F. Lu, D.-W. Fu and Q. Guo, Tunable phase transition temperature and nonlinear optical properties of organic–inorganic hybrid perovskites enabled by dimensional engineering, *J. Mater. Chem. C*, 2022, **10**, 16330–16336.
30 H.-Y. Zhang and R.-G. Xiong, 3D Narrow-Bandgap Perovskite Semiconductor Ferroelectric Methylphosphonium Tin Triiodide for Potential Photovoltaic Application, *Chem. Commun.*, 2023, **59**, 920–923.
31 R. K. Misra, B. E. Cohen, L. Iagher and L. Etgar, Low-Dimensional Organic–Inorganic Halide Perovskite: Structure, Properties, and Applications, *ChemSusChem*, 2017, **10**, 3712–3721.
32 Y.-Y. Gong, T. Zhang, J. Li, D.-W. Fu, Y. Zhang and H.-F. Lu, Structural Optimization and Property Tunability by Halogen Regulation in Zero-Dimensional Zinc Halide Organic–Inorganic Hybrid Materials, *Cryst. Growth Des.*, 2022, **22**, 6801–6808.
33 H. Gao, T. Zhang, M. M. Lun, J. Y. Li, H. F. Lu, D. W. Fu and Y. Zhang, Chlorine Substitution in Spirocyclic Derivatives Triggers SHG Response in Noncentrosymmetric Crystal, *Chem. – Asian J.*, 2022, **17**, e202200791.

34 P.-Z. Huang, H.-F. Ni, C.-Y. Su, M.-M. Lun, H.-F. Lu, D.-W. Fu and Q. Guo, Thermal-induced Ferroelastics in Two Lead-free Organic–inorganic Hybrid Perovskites, *CCS Chem.*, 2022, DOI: 10.31635/ccschem.022.202202332.

35 Z. C. Zhang, T. Zhang, C. Y. Su, M. M. Lun, Y. Zhang, D. W. Fu and Q. Wu, Competitive Dual-Emission-Induced Thermochromic Luminescence in Organic-Metal Halides, *Inorg. Chem.*, 2022, **61**, 13322–13329.

36 M. Ksiądzyna, V. Kinzhybalo, A. Bieńko, W. Medycki, R. Jakubas, C. Rajnák, R. Boča, A. Ozarowski, M. Ozerov and A. Piecha-Bisiorek, Symmetry-breaking phase transitions, dielectric and magnetic properties of pyrrolidinium-tetrahalidocobaltates, *Inorg. Chem. Front.*, 2022, **9**, 2353–2364.

37 J.-M. Gong, T. Shao, P.-Z. Huang, C.-Y. Su, M. Chen, D.-W. Fu and H.-F. Lu, Reversible Phase Transition and Second-Harmonic Response Based on a Zero-Dimensional Organic–Inorganic Hybrid Compound, *J. Phys. Chem. C*, 2022, **126**, 15274–15279.

38 D.-W. Fu, J.-X. Gao, W.-H. He, X.-Q. Huang, Y.-H. Liu and Y. Ai, High-T_c Enantiomeric Ferroelectrics Based on Homochiral Dabco-derivatives (Dabco = 1,4-Diazabicyclo[2.2.2]octane), *Angew. Chem., Int. Ed.*, 2020, **59**, 17477–17481.

39 Q. Wei, T. Chang, R. Zeng, S. Cao, J. Zhao, X. Han, L. Wang and B. Zou, Self-Trapped Exciton Emission in a Zero-Dimensional $(TMA)_2SbCl_5$·DMF Single Crystal and Molecular Dynamics Simulation of Structural Stability, *J. Phys. Chem. Lett.*, 2021, **12**, 7091–7099.

40 K.-J. Li, Y.-Y. Zhao, M.-E. Sun, G.-S. Chen, C. Zhang, H.-L. Liu, H.-Y. Li, S.-Q. Zang and T. C. W. Mak, Zero-Dimensional Zinc Halide Organic Hybrids with Excellent Optical Waveguide Properties, *Cryst. Growth Des.*, 2022, **22**, 3295–3302.

41 H. Y. Zhang, Z. X. Zhang, X. G. Chen, X. J. Song, Y. Zhang and R. G. Xiong, Large Electrostrictive Coefficient in a Two-Dimensional Hybrid Perovskite Ferroelectric, *J. Am. Chem. Soc.*, 2021, **143**, 1664–1672.

42 M. Szafrański, A. Katrusiak and K. StÅhl, Time-dependent transformation routes of perovskites $CsPbBr_3$ and $CsPbCl_3$ under high pressure, *J. Mater. Chem. A*, 2021, **9**, 10769–10779.

43 C. Su, M. Lun, Y. Chen, Y. Zhou, Z. Zhang, M. Chen, P. Huang, D. Fu and Y. Zhang, Hybrid Optical-Electrical Perovskite Can Be a Ferroelastic Semiconductor, *CCS Chem.*, 2022, **4**, 2009–2019.

44 R. Y. Ren, C. Y. Su, T. Shao, Z. X. Zhang, P. Z. Huang, Y. Zhang, Q. Q. Jia and D. W. Fu, Dehydration-activated structural phase transition in a two-dimensional hybrid double perovskite, *Dalton Trans.*, 2022, **51**, 7783–7789.

45 Y. Xie, Y. Ai, Y. L. Zeng, W. H. He, X. Q. Huang, D. W. Fu, J. X. Gao, X. G. Chen and Y. Y. Tang, The Soft Molecular Polycrystalline Ferroelectric Realized by Fluorination Effect, *J. Am. Chem. Soc.*, 2020, **142**, 12486–12492.

46 H.-P. Lv, W.-Q. Liao, Y.-M. You and R.-G. Xiong, Inch-Size Molecular Ferroelectric Crystal with a Large Electromechanical Coupling Factor on Par with Barium Titanate, *J. Am. Chem. Soc.*, 2022, **144**, 22325–22331.

47 J. Liu, L. J. Han, T. Shao, C. Y. Su, M. Chen, P. Z. Huang, Q. Q. Jia, D. W. Fu and H. F. Lu, Metal ion induced dual switchable dielectric and luminescent properties in hybrid halides, *Dalton Trans.*, 2022, **51**, 14408–14412.

48 Z. Tang, X.-F. Sun, Z.-R. Gao, S.-L. Jiao, W.-C. Tang, X.-M. Yang, H.-L. Cai and X. S. Wu, New Room-Temperature Molecular Ferroelectric $(C_6H_{16}N_2O)CdBr_4·H_2O$ with Preferable Luminescent Properties, *J. Phys. Chem. C*, 2022, **126**, 21126–21135.

49 K. Li, Z. G. Li, J. Xu, Y. Qin, W. Li, A. Stroppa, K. T. Butler, C. J. Howard, M. T. Dove, A. K. Cheetham and X. H. Bu, Origin of Ferroelectricity in Two Prototypical Hybrid Organic–Inorganic Perovskites, *J. Am. Chem. Soc.*, 2022, **144**, 816–823.

50 Y. Wang, T. Zhang, M.-M. Lun, F.-L. Zhou, D.-W. Fu and Y. Zhang, Halogen regulation triggers NLO and dielectric dual switches in hybrid compounds with green fluorescence, *Inorg. Chem. Front.*, 2021, **8**, 4230–4238.

51 P. Jain, A. Stroppa, D. Nabok, A. Marino, A. Rubano, D. Paparo, M. Matsubara, H. Nakotte, M. Fiebig, S. Picozzi, E. S. Choi, A. K. Cheetham, C. Draxl, N. S. Dalal and V. S. Zapf, Switchable electric polarization and ferroelectric domains in a metal-organic-framework, *npj Quantum Mater.*, 2016, **1**, 16012.

52 Z.-X. Zhang, T. Zhang, P.-P. Shi, W.-Y. Zhang, Q. Ye and D.-W. Fu, Exploring high-performance integration in a plastic crystal/film with switching and semiconducting behavior, *Inorg. Chem. Front.*, 2020, **7**, 1239–1249.

53 H. Peng, Q. Liu, Y. Liu, Y. Lu and W. Liao, A chiral lead-free tin(IV)-based halide organic–inorganic semiconductor with dielectric switching and phase transition, *Chin. Chem. Lett.*, 2022, DOI: 10.1016/j.cclet.2022.107980.

54 M.-M. Lun, T. Zhang, C.-Y. Su, J. Li, Z.-X. Zhang, D.-W. Fu and H.-F. Lu, A ferroelastic molecular rotator $[(Me_2N(CH_2)_2NH_3)$(18-crown-6)]triflate with dual dielectric switches, *Mater. Chem. Front.*, 2022, **6**, 1929–1937.

55 Y.-F. Gao, Z.-X. Zhang, T. Zhang, C.-Y. Su, W.-Y. Zhang and D.-W. Fu, Regulated molecular rotor in phase transition materials with switchable dielectric and SHG effect, *Mater. Chem. Front.*, 2020, **4**, 3003–3012.

56 X. You, J. Yao and Z. Wei, Tin based organic–inorganic hybrid semiconductors with reversible phase transition and dielectric anomaly, *Dalton Trans.*, 2020, **49**, 7252–7257.

57 S. Zhou, L. Zhou, Y. Chen, W. Shen, M. Li and R. He, Boosting Blue Emission of Organic Cations in a Sn(IV)-Based Perovskite by Constructing Intermolecular Interactions, *J. Phys. Chem. Lett.*, 2022, **13**, 8717–8724.

58 Y. Sui, W.-T. Chen, S.-X. Ouyang, W.-Q. Wang, G.-X. Zhang and D.-S. Liu, A Semiconducting Organic–Inorganic Hybrid Metal Halide with Switchable Dielectric and High Phase Transition Temperature, *J. Phys. Chem. C*, 2019, **123**, 9364–9370.

59 X.-N. Hua, J.-X. Gao, T. Zhang, X.-G. Chen, D.-S. Sun, Y.-Z. Zhang and W.-Q. Liao, Switchable Dielectric Phase Transition with Drastic Symmetry Breaking in a Sn(IV)-Based Perovskite-Type Halide Semiconductor, *J. Phys. Chem. C*, 2019, **123**, 21161–21166.

